Progress in Mediating Cell Functions on Honeycomb Substratum

Xiaohui Wu, Ph.D
Department of Biomedical Engineering, Case Western Reserve University, Wickenden Building, Room 419, 10900 Euclid Avenue, Cleveland, Ohio 44106-7207, USA
Email: xxw291@case.edu

Abstract
The clinic needs of advanced biomaterials for tissue regeneration have driven the study on pores, ridges, fibers, and other microstructured features to mimic the topographies available on basement membranes. Recently, the honeycomb topography with well-ordered pores has drawn increasing attention due to its significant influence on cell functions and the effects can be cell type dependent. To gain potential application in tissue regeneration, we have to obtain good understanding of the interaction between honeycomb pores and cells. In this review article, we will introduce the deep meanings of research on honeycomb topography, review several useful approaches to fabrication of honeycomb patterns, describe topographical influence on application in biomaterials, and discuss the regulation of cell function on honeycomb patterns.

Keywords: biomaterials, cell functions , honeycomb, , tissue regeneration.

Introduction

Basement membranes with complex structures of pores, ridges, fibers, and other microstructured features exist throughout vertebrate body and provide substrata for overlying cellular structures. They are composed of extracellular matrix (ECM) proteins such as fibrous collagen, laminin, and fibronectin, which supply integrin receptors for cell anchorage and regulate subsequent events [1,2]. Structural features at the micro- and nanometer scales, the main topography of basement membranes, the surface chemistry, and their mechanical properties dramatically affect integrin-cytoskeleton links and cell functions. When cells react to membrane surfaces, basement membranes modulate cell functions through the activation of plasma membrane integrin receptors, such as RGD binding to ligands available on the membrane [3,4]. In addition, integrin receptors are considered to be signaling molecules related to activation of intracellular pathways influencing cell behavior. Besides, cell receptors which are mechanochemical transducers regulate cell behavior by activating signal transduction pathways, which is mediated by both matrix rigidity and biochemical composition through strengthening cytoskeletal linkages [5]. Along with surface chemistry and mechanical properties, topography is believed to regulate cell functions through “contact guidance” [6-8]. Accordingly, it is of great importance to evaluate cell-biomaterial interaction regarding material chemistry, mechanical properties, and surface topography when scientists design promising medical implants and the production of pharmaceuticals. Synthetic substrates with grooves, pits, pores, wells and nodes, spheres, or ridges, have been developed to mimic these complex features and it has been experimentally demonstrated that physical topography plays an important role in guiding cell migration, cytoskeletal organization, adhesion, proliferation, and differentiation [9-11]. In the past decades, many attractive methods such as phase separation, colloidal templating, lithography, and breath-figure have been invented to fabricate porous topography with ordered structures and various cell functions have been evaluated on porous topography [12-16]. The purpose of this paper is to: (1) review several useful approaches to fabrication of honeycomb patterns, (2) describe topographical influence on application in

biomaterials, and (3) discuss the regulation of cell function on honeycomb patterns.

2. Approaches to Fabrication of Honeycomb Patterns

2.1 Phase Separation

Immiscible polymer blends dissolved in a common solvent present phase separation when the solvent evaporates. Phase separation can induce 2-dimensional or 3-dimensional structural features, such as bicontinuous structure, islands, and deep holes when the preparation conditions, such as composition, molecular weight, cast volume, solvent property, temperature, pressure, and substrate on which the phase separation occurs, are modulated [17-27]. Morphologies can be formed from film and bulklike phase separation, which are governed by different means. In film phase separation, the surface features available on the substrates and other exterior conditions play an important role in determining the polymer structure [28-31]. On the other hand, the morphologies from bulklike phase separation are mainly determined by thermodynamic equilibrium [32]. PS/PVP polymer blends cast on mica substrates from ethylbenzene solution formed honeycomb surface under certain air flow rate due to phase separation as shown in Figure 1 [27]. Disordered pores are observed when the air flow rate is very low (figure 1a and b), while highly ordered ones are observed when the air flow rate is 1.0 L/min. The diameters for weight ratios of 4/1 and 7/1 under air flow rate of 1.0 L/min were determined to be 2.5 and 2 μm, respectively. The rim sizes corresponding to weight ratios of 4/1 and 7/1 under air flow rate of 1.0 L/min were 3.8 and 3.0 μm, respectively. Apparently, the rim size is very large compared with pore diameter. However, the phase separation which occurs at solvent quenching process can form much relatively smaller rim size [33]. Poly(L-lactide) (PLLA) and Poly(ethylene glycol) (PEG) polymer blend in 1, 4-dioxane at 323 K could form honeycomb pattern perpendicular to the freezing direction through an unidirectional freezing process as shown in Figure 2. The structure parallel to the freezing direction presents microtubes. The honeycomb pores fabricated from phase separation normally are not interconnected.

2.2 Colloidal Templating

Templating methods have been widely applied for fabrication of honeycomb films with controllable structure, in which the colloidal particles work as template for creating 2-dimensional or 3-dimensional well-ordered pores [34-39]. In these methods, the voids between colloidal particles are filled with different materials and the colloidal particles are simple to be removed by either etching or thermal treatment, leading to highly ordered pores in the films. Although the pore size can be controlled by using template colloidal particles with various sizes, the pore size and rim size available on the film surface are not controllable. Due to the stack of multi-layer colloidal particles as template, multi-layer pores are usually observed in the films. In addition, interconnected pores are formed when the colloidal particles are packed closely.

2.3 Breath-Figure

Compared with other methods, the breath-figure method is more simple and economical, in which polymer is dissolved in a volatile and water-immiscible solvent such as chloroform ($CHCl_3$), benzene, and carbon disulfide (CS_2) and then the solution evaporates quickly in a humid environment. The sharp drop of the temperature in polymer solution upon rapid solvent evaporation causes condensation of water vapor in air. Subsequently polymer precipitates and stabilizes water droplets with identical diameters orderly packed in a hexagonal array on the solution/air interface as the result of capillary force and convection currents. Then honeycomb polymer films can be observed upon complete drying as shown in Figure 3. Generally, parameters which exert a significant impact on the porous structure include the type of volatile solvents, air flow rate, humidity, additives,

interfacial activity of polymers, and the concentration of polymer solution [40-43]. For example, water droplets tend to be immersed into solvents with lower density and induce the formation of multi-layer pores, while denser solvents support the formation of single-layer water droplets on the solution surface and induce single-layer pores. The evaporation can be promoted by airflow rate causing the formation of more water droplets and smaller pores are observed at higher airflow rate.

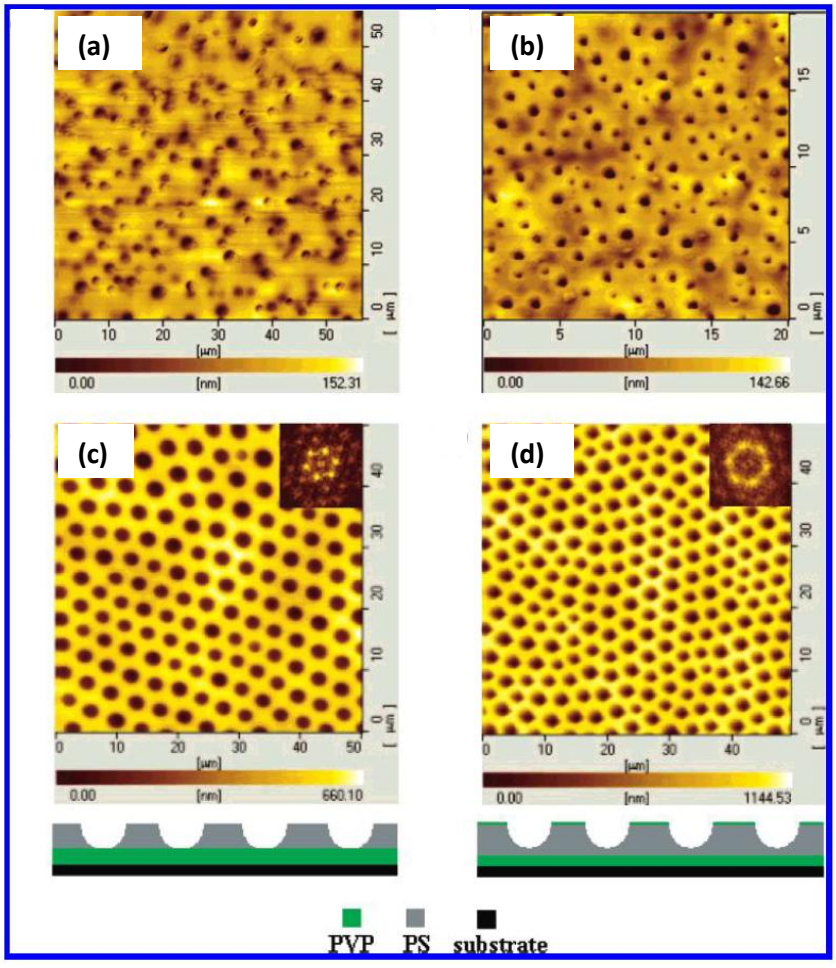

Figure 1. AFM images of PS/PVP films with weight ratio of 4/1 (a and c) and 7/1 (b and d) under low air flow rate (a and b) and 1.0 L/min (c and d). The bottom of panels c and d shows the corresponding possible structure. Reprinted with permission from ref. 27. Copyright 2014 American Chemical Society.

Although BF method is useful for fabricating honeycomb pores with controllable pore size, it has been widely employed to create honeycomb structure from limited categories of polymers, such as amphiphilic copolymers, rod-coil block copolymers, and star polymers [44]. Especially in biomedical field, researchers fabricated various honeycomb films using BF method for amphiphilic copolymers, or polymers with assistance of surfactants in

water-immiscible solvents. Recently, honeycomb PLLA and polycaprolactone (PCL), which are homopolymers, films have been fabricated without assistance of surfactants using water-miscible solvent, THF, and the pore size can be tuned by the humidity of the atmosphere, solution concentration, molecular weight, and air flow rate [25,45].

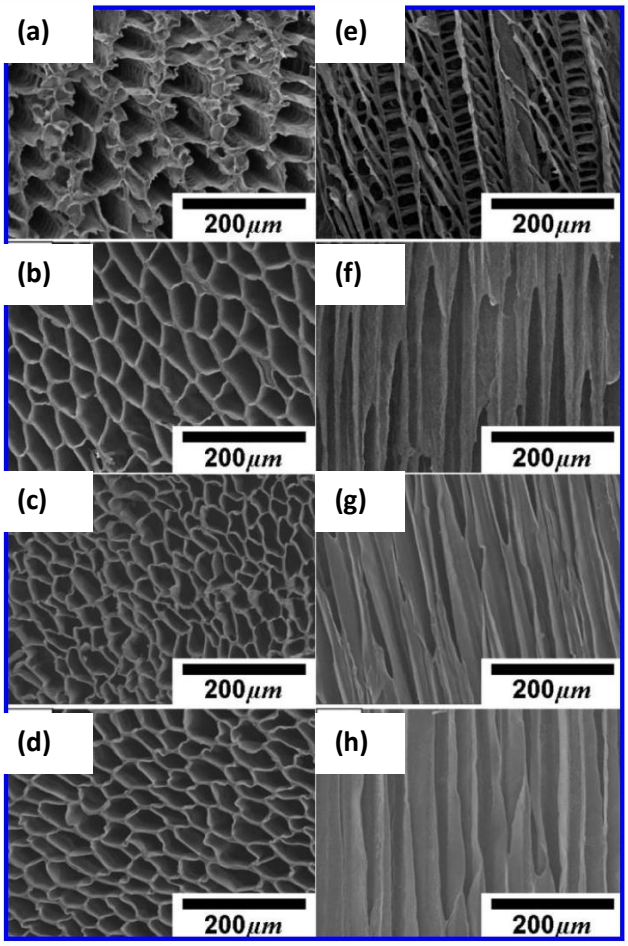

Figure 2. SEM images of honeycomb patterns fabricated from PLLA/PEG blend (90/10): (a-d) cross-sectional area perpendicular to the freezing direction, (e-h) cross-sectional area parallel to freezing direction, (a,e) PEG600, (b,f) PEG2000, (c,g) PEG4000, and (d,h) PEG6000. Reprinted with permission from ref. 33. Copyright 2014 American Chemical Society.

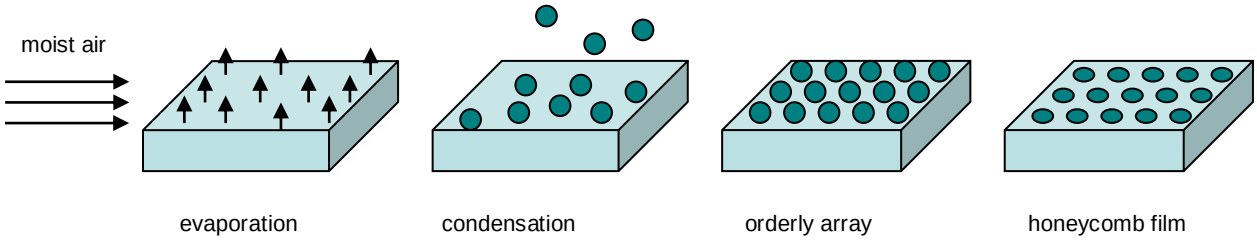

Figure 3. Mechanism of Breath-Figure method

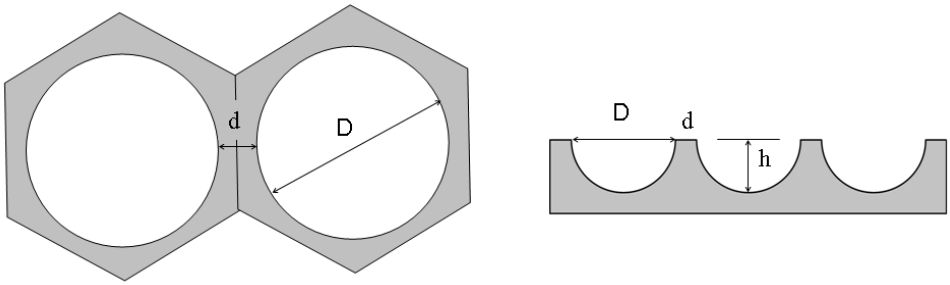

Figure 4. Model of two adjacent hexagonal unit cells containing pores and schematic cross-sections of films. D, d, and h represent pore diameter, rim size, and depth, respectively.

3. Topographical influence on properties of biomaterials.

In most situations, the honeycomb films with regular hexagonal unit cells containing pores can be fabricated, particularly in case of colloidal templating and BF methods. The geometrical feature of honeycomb pores can be illustrated as in Figure 4. The formation of pores plays an important role in physical properties determining the applications, such as separation, catalysts, tissue engineering, and the field of electrical materials. Regarding the application in biomaterials, we, here, discuss how pore diameter (*D*), rim size (*d*), and pore depth (*h*) influence specific surface area of films, the ratio of total surface area to the projected area, the water contact angles on these films, namely, wettability, and region of junction or discontinuity.

With the formation of large number of pores, the specific surface area of honeycomb films increases dramatically compared with flat surface and can be varied with pore size. In the study of honeycomb PCL films fabricated through BF method, the surface area increased from 1.15 ± 0.11 to 2.03 ± 0.18 when the pore diameter (*D*) decreased from 10 μm to 3.5 μm [45]. From the view of geography, the surface area can be larger when the pores are stacked closer to each other, the pore depth (*h*) is higher, and the rim size (*d*) is smaller.

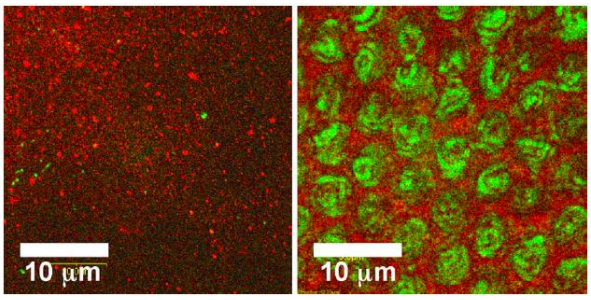

Figure 5. Fluorescence images of adsorbed protein on flat films (left) and honeycomb films (right). Green and Red points indicated fibronectin and albumin, respectively. Reprinted with permission from ref. 46. Copyright 2014 Elsevier.

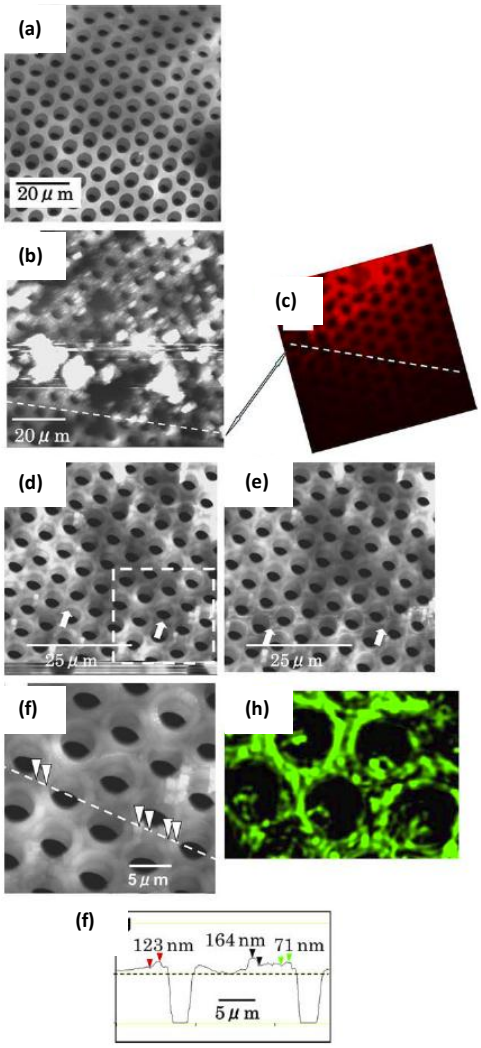

Figure 6. AFM and CLSM images of the morphology of adsorbed fibronectin as a function of incubation time in a PBS solution containing Fn. (a) AFM image before incubation. (b) AFM image at 20 h incubation time. (c) CLSM image at 20 h incubation time. The dashed line represents the boundary separating two domains having different morphology and fluorescence intensity. (d) AFM image at 48 h incubation time. (e) AFM image of surface after several scans on the surface shown in (d), showing that ring-like structure of Fn were scraped off by the AFM tip by comparing the areas with white arrow indication. (f) AFM image of area enclosed by dashed line in (d). (g) Cross-sectional profile along dotted line in (f). (h) CLSM image at 48 h incubation time. Reprinted with permission from ref. 47. Copyright 2014 Elsevier.

The formation of pores on the surface also exerts an important impact on protein adsorption. The study on honeycomb PCL films indicated that the amount of serum proteins in α-MEM employed for MC3T3-E1 cell culture was increased with decreasing the pore diameter, namely, increasing the specific surface area [45]. In addition, the protein adsorption presented linear relationship with specific surface area. The results in another study as shown in Figure 5 revealed that honeycomb films adsorbed more fibronectins (Fn) than flat films and the fibronectins were mainly located inside the pores [46]. On the other hand, the adsorption of albumin was non site-

selective on honeycomb and flat films. In addition, the honeycomb morphology can also influence the structural transition of fibronectin [47]. Due to the fact that protein molecules bound to a surface can rearrange through conformational changes and diffusion, they can form 3-dimensional aggregates. As shown in Figure 6, both AFM and confocal laser scanning microscope (CLSM) images indicated that Fn displayed a structural transition from globular form on the rim of the film to ring form around the pore edges, which can be ascribed to the self-organization of Fn induced by the dependence of diffusion on the surface morphology. Similarly, it is also reported that Fn adsorption was regulated on Au/Si patterns, in which Fn was adsorbed on the Si domains but repulsed by the Au domains, resulting in the Fn organization determined by Si domains [47].

The wettability of polymer films could be sharply influenced by surface topography [48-50]. To create higher hydrophobicity, the critical point is how to form stable interface with air pockets between substrate surface and water droplets. Micro- or nano-structured surface could produce air pockets when the size of water droplets was much larger than the dimension of structures present on substrate surface. Honeycomb films caused the formation of air pockets between surface and water droplets. Hence, the Cassie and Baxter model (eq. 1) could be employed to predict water contact angles on these films.

$$\cos\theta = R_f - f_{LA}(R_f \cos\theta_0 + 1) \qquad (1)$$

Where f_{LA} is the fractional flat geometrical area of liquid-air interface beneath water droplet, R_f is a roughness factor defined as the ratio of the solid-liquid area to its projection on a flat plane, θ_0 is the water contact angle on smooth surface. For honeycomb PCL films, when the pore diameters were 10, 6.0 and 3.5 μm, the rim sizes were measured to be 3.05 ± 0.25, 1.71 ± 0.40 μm, and 0.83 ± 0.04 μm, respectively. f_{LA} were calculated to be 0.528, 0.553, and 0.592, respectively. The contact angles calculated from eq. 1 were 112.6°, 114.6°, and 117.9, respectively. Experimentally the water contact angles were measured to be 72.6 ± 1.8°, 104.0 ± 1.5°, 113.5 ± 2.1°, and 136.4.0 ± 4.4° on the flat films and honeycomb films with pore diameters of 10, 6.0 and 3.5 μm, respectively. Although the prediction was not perfectly consistent with experimental values, it provided reasonable explanation for contact angle results. However, another study on honeycomb PCL films revealed different results [51]. The water contact angles were measured to be 105.6 ± 1.64°, 104.3 ± 3.73°, 107.2 ± 1.48°, and 105.0 ± 3.86° without prominent difference among honeycomb PCL films with pore diameters of 5.3 ± 0.02 μm, 9.1 ± 0.03 μm, 11.8 ± 0.15 μm, and 15.6 ± 0.08 μm, respectively. The main reason for this opposite phenomenon might be the difference of honeycomb structures, such as rim size (*d*) and related f_{LA} values.

Moving or extending cells preferred to be localized at the region of junction or discontinuity [45,52]. In case of honeycomb pores, the junction or discontinuity are the pore edges on the honeycomb films. Based on the f_{LA} and D values, the number of pores and the total length of pore edges in a unit projected area can be estimated. In the study on honeycomb PCL films, the number of pores in a unit projected area of 1 cm^2 increased from 6.8×10^5 to 1.9×10^6 and 6.2×10^6 when pore size decreased from 10 to 6.0 and 3.0 μm, respectively. The total length of pore edges in a unit projected area of 1 cm^2 increased from 21.3 to 36.6 and 67.7 m when pore size decreased from 10 to 6.0 and 3.0 μm, respectively. Hence, honeycomb films provide more junction or discontinuity for cell adhesion and growth.

4. Regulation of cell function on honeycomb patterns

Most tissue-derived cells fall into the category of anchorage dependent cells and cell attachment to the material surface in the early stage is of importance for cell viability and growth, which determine subsequent events, such as cell spreading, proliferation, and differentiation. During cell attachment, especially for anchorage dependent cells, the surface properties, such as chemistry, topography, and mechanical

properties, play an important role. As we discussed in previous section, the formation of pores changes the topography of films and subsequent properties regarding biology, such as protein adsorption, wettability, and disconnuity, which exert huge influence on cell functions. By evaluating their impact on cell functions, such as adhesion, spreading, proliferation, and differentiation, we are able to investigate their potential application in tissue engineering.

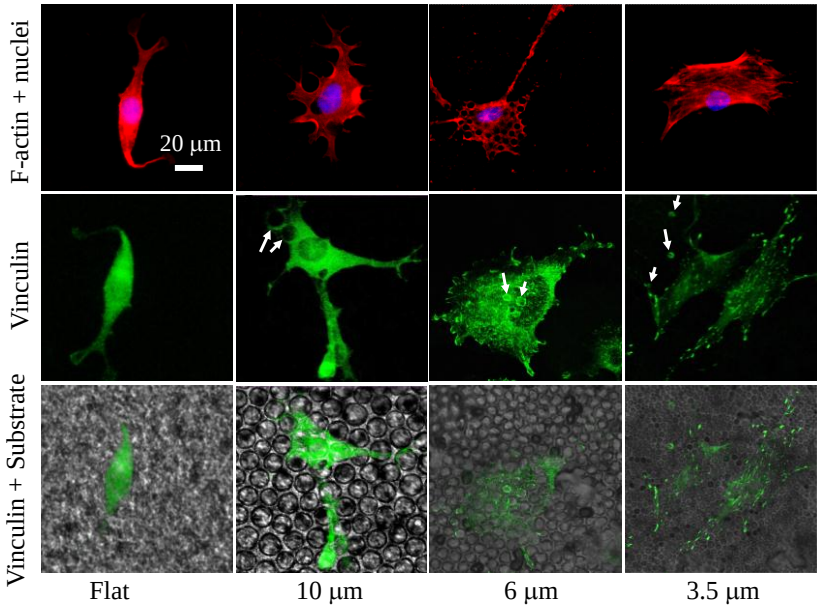

Figure 7. Fluorescent images of MC3T3-E1 cells stained with RP (red) and DAPI (blue) (top row), vinculin-stained cell images (middle row) with arrow heads indicating pores of the honeycomb films, and merged images with the underlying substrates at day 1 post-seeding. Scale bar of 20 μm is applicable to all. Reprinted with permission from ref. 45. Copyright 2014 American Chemical Society.

4.1 Bone cells

In this review, we focus on the study on MC3T3-E1, OCT-1, and chondrocyte cell function on honeycomb films. MC3T3-E1 cells could spread over multiple pores without being aligned along the rim as shown in Figure 7 [45]. Cytoskeleton on the flat films had very few stress fibers while the cells on the honeycomb films spread better and had more stress fibers and protrusions. When the pore diameter was larger than 6.0 μm, the cytoskeleton on the honeycomb films was trapped inside the pores. Vinculin-staining images in Figure 7 showed that there were significantly more punctate focal adhesions (FAs) on the honeycomb films, especially when the pore size became smaller, in contrast to diffusive vinculin staining on the flat ones. In addition, the pores influenced the FA morphology. The FAs on the honeycomb films were located not only on cell periphery but also along the pore edge. The statistical analysis for FAs, such as the average area of FAs, FA density defined as the average number of FAs per cell, and the circularity of FAs, defined as $4\pi \times \text{area/perimeter}^2$ demonstrated that the average area and density of FAs on the honeycomb films were markedly larger than those on the flat ones and were further strengthened by decreasing the pore size. The circularity of FAs was lower on the honeycomb films and decreased with the decrease of pore size, indicating that the alignment of FAs was enhanced on smaller pores. Integrins, transmembrane heterodimers of the α-subunit and β-subunit, play a great role in determining

the FA-ECM interactions, in which integrins can bind different ECM proteins with the external end and cytoskeleton through adapter proteins, such as talin, α-actinin, filamin, and vinculin, and FAs are based on this integrin-adapter protein–cytoskeleton complex. Osteoblasts anchor on substrate surface by integrin receptors involved in processes called "outside-in-signaling" and "inside-out-signaling" between the ECM and the cell. These integrin-involved pathways are of importance in regulating cell adhesion, migration, proliferation, and differentiation. The expression levels of integrin subunits α_1, α_2, and β_1 on the honeycomb films with smaller pores were significantly higher than on flat ones, especially when the pore size decreased. Accordingly, the cell proliferation and differentiation on honeycomb PCL films, especially with smaller pores, were also enhanced compared with flat films.

Protein adsorption, dependent on material chemistry and morphology, exerts an important impact in cell adhesion. Honeycomb films with larger specific surface area could promote protein adsorption from serum media employed for cell culture compared with flat films and smaller pores providing larger specific surface area supported better protein adsorption, which might be reasonable explanation for better cell adhesion on honeycomb films. However, MC3T3-E1 cells did not grow inside for most pores, especially when the pore size was smaller than 6.0 μm. In another word, the better protein adsorption on honeycomb films might not contribute much to better cell adhesion on honeycomb films. Also, it is suggested, as discussed earlier, that honeycomb structures not only enhanced protein adsorption but also influenced distribution of adsorbed proteins [46,47,53]. For instance, the fibril-like aggregates of fibronectin were observed on the periphery of the pores of honeycomb PCL films, which might further influence the FAs around these pores.

In addition to that honeycomb films enhanced cell adhesion, proliferation, and differentiation, the nuclei morphology was also significantly influenced by pores as shown in Figure 8. Cell nuclei became larger on the honeycomb films and were evidently distorted on the 6.0- and 10-μm pores when cytoplasm was trapped inside the pores. This kind of nuclear deformation might contribute to better difference expression of bone-specific gene markers on honeycomb films.

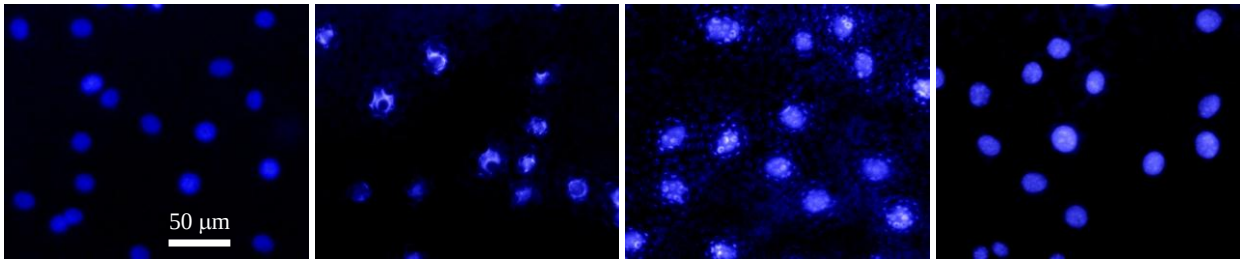

Figure 8. MC3T3-E1 cell nuclei with DAPI staining (blue) at day 2 post-seeding on the flat film and honeycomb films with various pore size. Reprinted with permission from ref. 45. Copyright 2014 American Chemical Society.

Silica films with pore diameters (100, 300, 500, and 1000 nm) were also employed to investigate the MC3T3-E1 cell behavior on ordered nanometer-sized pores [54]. On the contrary, silica films with 100-500 nm pores inhibited cell growth and induced lower cell adhesion compared with flat silica films or films with 1000 nm pores. It seems that the optimal pore size for MC3T3-E1 cells is 1~3.5 μm, at smaller or larger size than this range the cell functions will be

inhibited. However, the first study used polymer, PCL, to evaluate cell behavior, whereas the other one employed inorganic materials, silica. The materials with different physical and chemical properties might influence cell behavior in a different manner. Consequently, it is unclear how MC3T3-E1 cells respond to nanometer-sized pores on PCL films. They might follow the same way as the case for nanometer-sized silica films, however, the response can also be totally different.

OCT-1 osteoblast-like cells also showed different behavior on micro-scale and nano-scale pits of the polystyrene (PS) films from that of MC3T3-E1 cells on honeycomb PCL films [55]. Even though OCT-1 cells showed higher cell attachment efficiency on micro- and nano-pits PS than on smooth PS, which might be ascribed to the enlargement of the contact area of cells on pits-patterned PS, they did not show distinct difference in proliferation, which is in contrast with the proliferation of MC3T3-E1 cells on honeycomb PCL films. Due to the huge difference in surface topography between pits-patterned PS and honeycomb PCL films, such as distribution of pore size, rim size, and pore depth, it is unclear that what factors caused this difference in cell response.

In another study, chondrocytes were cultured on honeycomb poly(lactic acid) (PLA) films to evaluate the effects of pores on chondrocytes [56]. The results indicated that flat PLA films compared with honeycomb ones supported significantly higher levels of chondrocyte growth. However, chondrocytes on honeycomb films produced abundant extracellular matrix (ECM).

4.2 Neural stem/progenitor cells (NPCs/NSCs)

Even though some clinic treatments for the injuries of the peripheral nervous system (PNS) and central nervous system (CNS) have been achieved via end-to-end surgical reconnection of the severed nerve ends and autologous nerve graft [57]. However, both approaches have severe limitations. For example, end-to-end reconnection treatment can, to date, be used to repair nerve injuries with small gaps but not long gaps [57-59]. As a result, the tremendous needs of advanced therapies and devices have driven the development of promising synthetic biomaterials for nerve regeneration. Physically, an advanced biomaterial for nerve regeneration should strengthen not only proliferation of nerve cells but also axon extension across the lesion site bridging the gaps to achieve functional recovery. In this section, we describe the regulation of neural stem/progenitor cells on honeycomb films.

Neural stem cells (NSCs) were investigated on honeycomb PCL films, fabricated with assistance of amphiphilic copolymer, with different pore diameters (3, 5, 8, 10, and 15 μm) [60]. Honeycomb films supported higher cell viability and growth for neural stem cells, which has trend similar to that for MC3T3-E1 cells. The interesting point is that pores on the surface suppressed the differentiation of neural stem cells. The immunostaining images for nestin and MAP2 at day 4 post-seeding demonstrated that NSCs maintained undifferentiated state on honeycomb PCL films with pore diameter of 3 μm as shown in Figure 9. Even though some cells were positive for Nestin and MAP2 on honeycomb PCL films with pore diameters of (5, 8, 10, and 15 μm) as shown in Figure 10, the differentiation was better on flat films than honeycomb films. The differentiation degree was pore size dependent and increased with increasing the pore diameter. However, some important neurite characterizations, such as neurite length and the number of neurites per cell, were not provided in this study. The immunostaining images in Figure 9 and 10 prominently indicated that neurites on honeycomb films were longer along the pore edge direction compared with flat films, indicating better neurite extension.

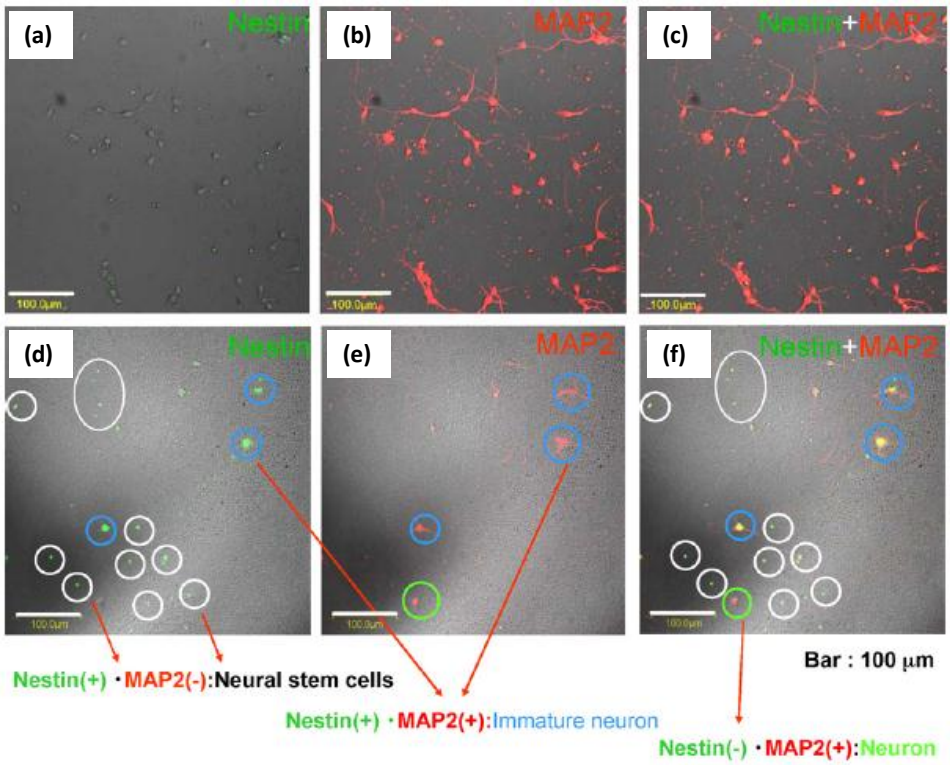

Figure 9. Immunostaining for Nestin and MAP2 on flat and honeycomb films (3 μm). (a) Nestin, (b) MAP2, and (c) Merge of Nestin and MAP2 staining on flat films. (d) Nestin, (e) MAP2, and (f) Merge of Nestin and MAP2 staining on honeycomb films (3 μm). Scale bar (100 μm) is applicable to all images. Reprinted with permission from ref. 60. Copyright 2014 Elsevier.

During neuronal polarization through the generation of long cellular protrusions from cells, namely, neurites, the topography of substrates provides significant guidance for formation and stabilization of FAs which dominate the neurite initiation and outgrowth [61-63]. The neurites grow and proceed toward specific targets in a process called pathfinding [64]. The efficient neurite alignment was observed on nanogratings with dimension of 500 nm in linewidth and 350 nm in depth [62]. Consequently, we have two points regarding NPC/NSC differentiation on honeycomb films to propose. Firstly, the rims surrounding pores on the honeycomb films can be considered as circular groove ridges, which might provide the topographical guidance during neurite outgrowth. However, due to the inflexible characteristic of the microtubules and actin filaments binding NPCs/NSCs, the neurite pathfinding can only develop in one or two directions [58], which might cause imperfect alignment along the pore rim. Secondly, the mechanism of how honeycomb pores affect cell-cell interaction and the differentiation of NPCs/NSCs into highly specialized cells, such as astrocytes, mature neurons, immature neurons, and oligodendrocytes is still unknown.

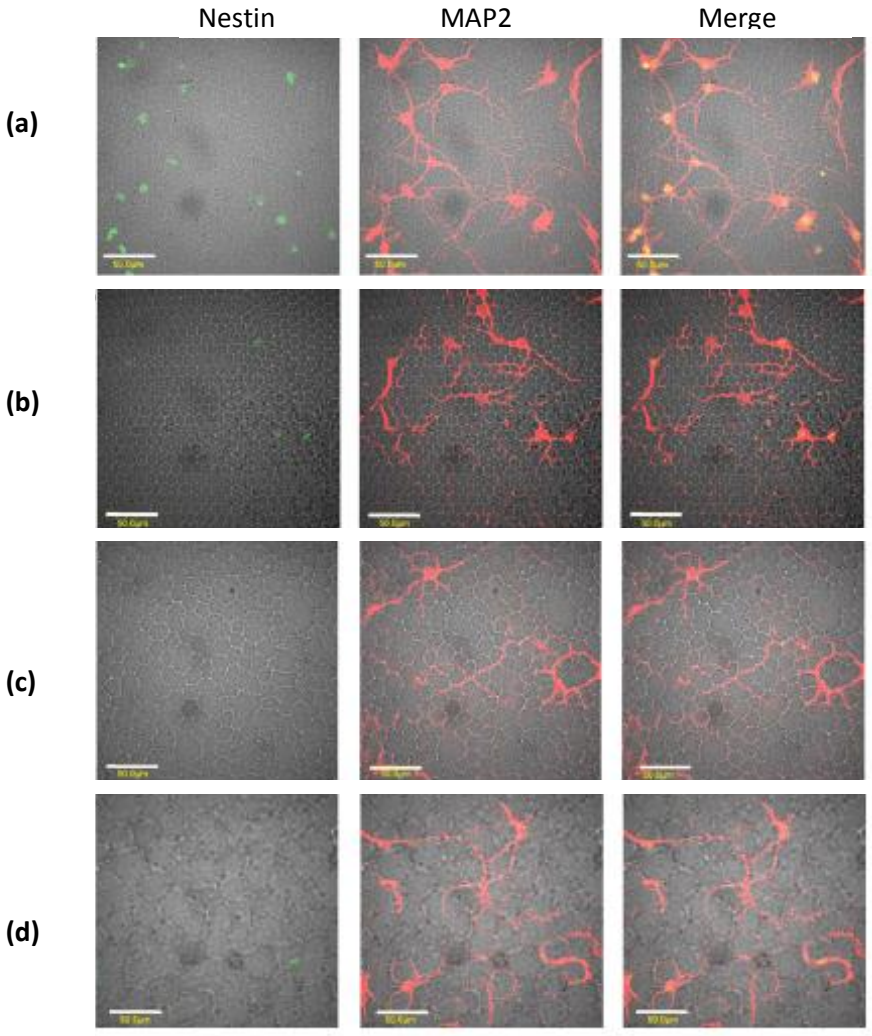

Figure 10. Immunostaining for Nestin and MAP2 on flat films and honeycomb films at day 4 post-seeding. (a) 5 μm, (b) 8 μm, (c) 10 μm, and (d) 15 μm. Scale bar (50 μm) is applicable to all. Reprinted with permission from ref. 60. Copyright 2014 Elsevier.

4.3 Skin cells

Endothelial cells (ECs) were seeded on flat PCL films and honeycomb PCL films fabricated with assistance of amphiphilic copolymer with a diameter of 5 μm [46]. The FAs of ECs on honeycomb films were mainly located inside the honeycomb pores, whereas the FAs of ECs on flat films did not show preferential site-distribution. Meanwhile, the images in Figure 11 also clearly demonstrated that ECs spreaded over pores on honeycomb films with larger area than on flat ones. Because of better cell adhesion on honeycomb films than on flat ones, the cell number of ECs on honeycomb films was four times larger than that on flat ones.

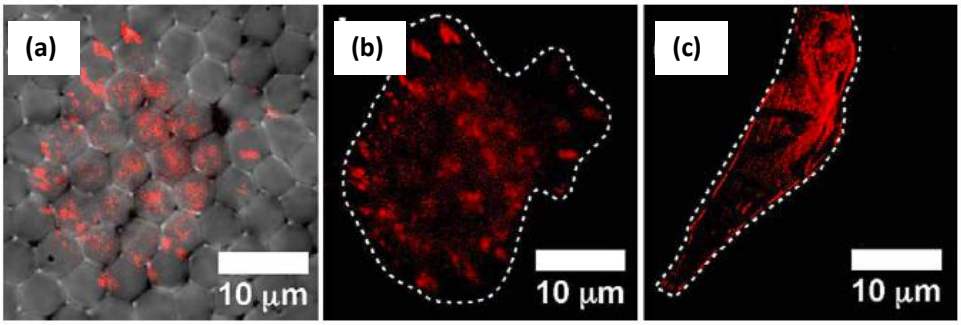

Figure 11. (a) Superposition image of differential interface image and vinculin-stained image (red). FAs stained with vinculin (red) on (b) honeycomb films and (c) flat films. Reprinted with permission from ref. 46. Copyright 2014 Elsevier.

The cell behavior of epidermal keratinocyte and dermal fibroblast cells was also investigated on honeycomb and flat PCL films [53]. Those two cell types responded to honeycomb films (pore diameters: 3 μm, 5 μm, and 10 μm) differently. Keratinocytes could adhered to the both flat and honeycomb films with thin filopodia projecting from the cell bodies and were more sensitive to the pore size than dermal fibroblast cells. Cells presented best spreading and adhesion on honeycomb PCL films with diameter of 3 μm, whereas they formed thick cell bodies distributed on the 5 μm surface with poorer spreading. On the 10 μm PCL films, the cell formed "fried egg" morphology covering the underlying pores. The cell-cell communication played an important role in cell growth, signaling, and survival of keratinocytes. When the pore diameter is larger than the initial dimension of cells, they can be trapped inside the film pore limiting cell communication with adjacent cells. This phenomenon has also been demonstrated that keratinocytes failed to generate epidermal sheets on grafts because of poor cell-cell and cell-substrate contact [65]. Consequently, cell spreading and adhesion were inhibited on 5 μm and 10 μm PCL films compared with 3 μm PCL films. In addition, smaller pore diameter provided larger length of pore edge per unit area and supported better plasma membrane lamelapodia and filopodia attaching the pores and inducing better cell adhesion, however, lowering cell migration. On the other hand, fibroblasts attached and spread on flat PCL films more quickly than on honeycomb ones, even though cells eventually formed flattened shape on honeycomb films.

4.4 Hepatocyte

Hepatocytes were cultured on flat and honeycomb amphiphilic copolymers consisting of dodecylacrylamide and ω-carboxyhexylacrylamide [66]. As shown in Figure 12, the hepatocytes spreaded on the flat films with thinner thickness than on honeycomb films, indicating better cell spreading on flat films. Meanwhile, the typical hepatocyte morphology, namely spheroids, was observed on honeycomb, which demonstrated that pores on honeycomb films inhibited cell spreading, even though cells still adhered to the surface. The study suggested that honeycomb films promoted the rapid formation and outgrowth of spheroids, expected to have better and longer hepatic function. This aspect is different from the observation for MC3T3-E1 cells, which preferred to spread on honeycomb films [45]. Consequently, the manner to regulating cell function on honeycomb films is cell type dependent and there is no universal conclusion for all cells. CLSM images in Figure 12 c and d showed that the actin filaments were conspicuous in hepatocytes on flat films, whereas the actin filaments were located in the intracellular edge with prominent formation of

small protrusions around the spheroids. It is proposed that the topographical feature available on the honeycomb films plays a role in signal transduction with the Rho family of small GTPase, which regulated the actin cytoskeleton, cell adhesion, and gene transcription [67]. As discussed above, honeycomb films provide a promising strategy for advanced biomaterials in bioartificial liver tissue engineering. However, the mechanism of how hepatocytes interact with honeycomb feature is still unclear.

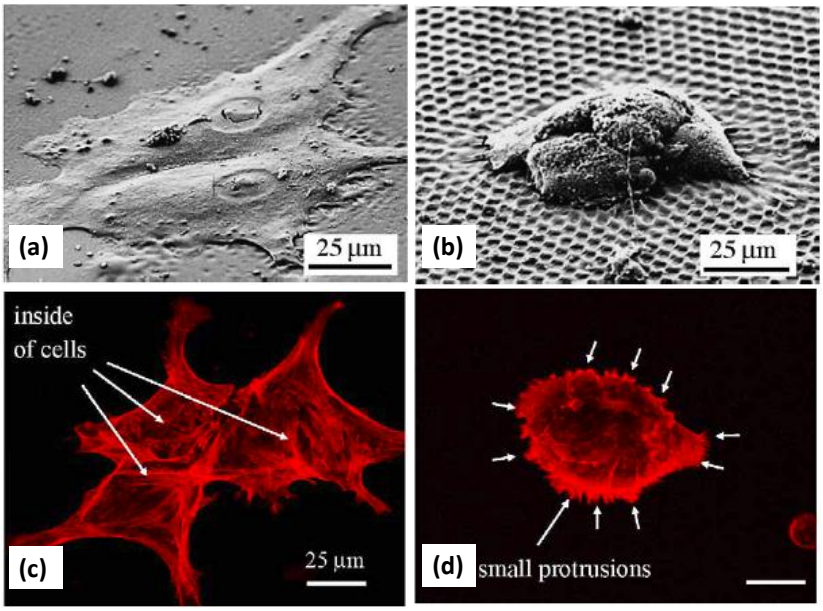

Figure 12. (a,b) SEM images and (c,d) CLSM images of hepatocytes stained with rhodamine-phalloidin (red) on flat films (a,c) and honeycomb films (b,d) at 72 h post-seeding. White arrows in (c) indicate inside of cells and white arrows in (d) indicate the localization of cell protrusions projected from cell body. Scale bar (25 μm) is applicable to all images. Reprinted with permission from ref. 66. Copyright 2014 Elsevier.

4.5 Fibroblast cells

Consistent with previous study on MC3T3-E1 cells on PCL films, human fibroblasts can adhere to and spread on honeycomb PCL films [68]. The honeycomb PCL films were fabricated using silica microspheres as template with a diameter of 5 μm. The SEM images clearly demonstrated that pores could trap cytoplasma partly and caused structural defect available in cell body. The authors attributed the crack of cell bodies to the vacuum treatment for SEM observation during which the air trapped inside the pore induced the crack. The MTT assay for quantifying cell number from day 2 to day 8 post-seeding showed that honeycomb PCL films enhanced cell proliferation compared with smooth surface. NIH3T3 fibroblast cells were seeded on honeycomb poly(D,L-lactide) (PLA) films with a diameter of 3 μm, which were fabricated with assistant of dioleoylphosphatidylethanolamine (DOPE) or a copolymer (CAP) of dodecylacrylamide and ω-carboxyhexylacrylamine [69]. As shown in Figure 13, NIH3T3 cells covered the surface of honeycomb films (PLA-2%DOPE), indicating excellent cell proliferation. The surface of honeycomb films (PLA-0.5%DOPE) was partly covered by NIH3T3 cells and cells migrated into the pores and adhered to the pore bottom with fiber-like extracellular matrices. On the contrary, less surface of honeycomb films (PLA-10%CAP)

were covered with cells which did not show clear fiber-like extracellular matrices compared with honeycomb films (PLA-0.5%DOPE). The cell proliferation calculated by alamar-Blue™ assay demonstrated that honeycomb films (PLA-2%DOPE) supported better proliferation than honeycomb films (PLA-10%CAP) and it was prominently better on honeycomb films (PLA-0.5%DOPE) than on these (PLA-2%DOPE). The results revealed that DOPE, one of the major building blocks of the cell wall possessed better biocompatibility than CAP which might be degraded into acrylamine and other moieties with potential toxicity to cells. However, the comparison between flat surface and honeycomb surface has not been made and it is unclear that honeycomb patterns inhibited or enhanced NIH3T3 cell functions.

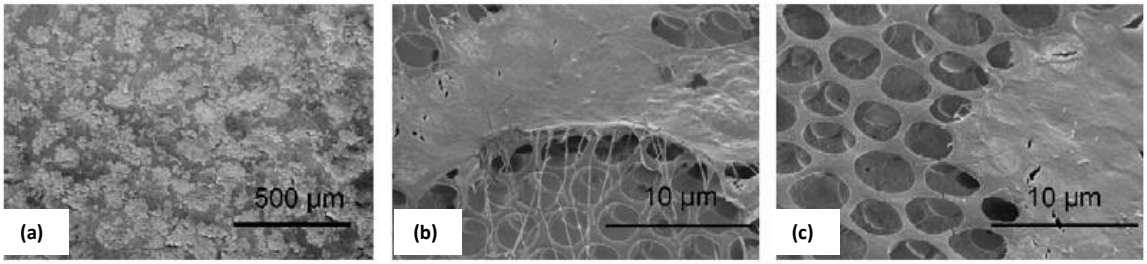

Figure 13. (a) SEM images of NIH3T3 cells on honeycomb films (PLA-2%DOPE), (b) FE-SEM image of NIH3T3 cells on honeycomb films (PLA-0.5%DOPE), and (c) FE-SEM image of NIH3T3 cells on honeycomb films (PLA-10%CAP) at day 14 post-seeding. 2%, 0.5%, and 10% represent the weight percentage of DOPE or CAP in honeycomb films. Reprinted with permission from ref. 69. Copyright 2014 Elsevier.

5. Conclusion

Honeycomb films can be fabricated through traditional or advanced technology, some of which render controllable pore dimension. These honeycomb films exert a significant influence in regulating cell functions with cell type-dependent response and have promising potential to obtain wide application in tissue engineering. However, there still exist some unclear problems, such as the mechanism how NSC/NPC cell functions are influenced by pore size, and how pores at nanometer scale influence cell functions. Consequently, more investigations are needed to have better understanding of cell behavior on honeycomb films, which provides promising support for wide applications in tissue engineering.

References

(1) Coopman, P. J.; Bracke, M. E.; Lissitzky, J. C. J. Cell. Sci. 1991, 98, 395.
(2) Flemming, R. G.; Murphy, C. J.; Abrams, G. A.; Goodman, S. L.; Nealey, P. F. Biomaterials 1999, 20, 573.
(3) Ruoslahti, E. Science 1997, 276, 1345.
(4) Clark, E. A.; Brugge, J. S. Science 1995, 268, 233.
(5) Choquet, D.; Felesenfiled, D. P.; Sheetz, M. P. Cell 1997, 88, 39.
(6) Curtis, A. S. G.; Clark, P. Crit. Rev. Biocompatability 1990, 5, 343.
(7) Rosenberg, M. D. Science 1963, 139, 411.
(8) Wu, X.; Wang, S. Adv. Healthc. Mater. 2013, 2, 326.
(9) Anselme, K.; Bigerelle, M.; Noel, B.; Iost, A.; Hardouin, P. J. Biomed. Mater. Res. 2002, 60, 529.
(10) Curtis, A.; Wilkinson, C. Trends. Biotechnol. 2001, 19, 97.

(11) Wilkinson, C. D. W. Microelectron. Eng.1995, 27, 61.
(12) Campbell, M.; Sharp, D. N.; Harrison, M. T.; Denning, R. G.; Turberfield, A. J. Nature 2000, 404, 53.
(13) Holland, B. T.; Blanford, C. F.; Stein, A. Science 1998, 281, 538.
(14) Zalusky, A. S.; Olayo-Valles, R.; Wolf, J. H.; Hillmyer, M. A. J. Am. Chem. Soc. 2002, 124, 12761.
(15) Widawski, G.; Francois, B. Nature 1994, 369, 387.
(16) Francois, B.; Pitois, O.; Francois, J. Adv. Mater. 1995, 7, 1041.
(17) Budkowski, A.; Bernasik, A.; Cyganik, P.; Raczkowska, J.; Penc, B.; Bergues, B.; Kowalski, K.; Rysz, J.; Janik, J. Macromolecules 2003, 36, 4060.
(18) Muller-Buschbaum, P.; Gutmann, J. S.; Stamm, M. Macromolecules 2000, 36, 4886.
(19) Affrossman, S.; O'Neill, S. A.; Stamm, M. Macromolecules 1998, 31, 6280.
(20) Kikuchi, T.; Kudo, M.; Jing, C.; Tsukada, T.; Hozawa, M. Langmuir 2004, 20, 1234.
(21) Harris, M.; Appel, G.; Ade, H. Macromolecules 2003, 36, 3307.
(22) Walheim, S.; Boltau, M.; Mlynek, J.; Krausch, G.; Steiner, U. Macromolecules 1997, 30, 4995.
(23) Gutmann, J. S.; Muller-Buschbaum, P.; Stamm, M. Appl. Phys. A. Mater. 2002, 74, S463.
(24) Woodcock, S. E.; Chen, C. Y.; Chen, Z. Langmuir 2004, 20, 1928.
(25) Newby, B. M. Z.; Composto, R. J. Macromolecules 2000, 33, 3274.
(26) Karim, A.; Slawecki, T. M.; Kumar, S. K.; Douglas, J. F.; Satija, S. K.; Han, C. C.; Russell, T. P.; Liu, Y.; Overney, R.; Sokolov, O.; Rafailovich, M. H. Macromolecules 1998, 31, 857.
(27) Cui, L.; Han, Y. Langmuir 2005, 21, 11085.
(28) Boltau, M.; Walheim, S.; Mlynek, J.; Krausch, G.; Steiner, U. Nature 1998, 391, 877.
(29) Krausch, G.; Kramer, E. J.; Rafailovich, M. H.; Sokolov, J. Appl. Phys. Lett. 1994, 64, 2655.
(30) Nisato, G.; Ermi, B. D.; Douglas, J. F.; Karim, A. Macromolecules 1999, 32, 2356.
(31) Cyganik, P.; Bergues, A.; Budkowski, A.; Bergues, B.; Kowalski, K.; Rysz, J.; Lekki, J.; Lekka, M.; Postawa, Z. Vacuum 2001, 63, 307.
(32) Tanaka, K.; Takahara, A.; Kajiyama, T. Macromolecules 1996, 29, 3232.
(33) Kim, J. W.; Taki, K.; Nagamine, S.; Ohshima, M. Langmuir 2009, 25, 5304.
(34) Deutsch, M.; Vlasov, Y. A.; Norris, D. J. Adv. Mater. 2000, 12, 1176.
(35) Jiang, P.; Hwang, K. S.; Mittleman, D. M.; Bertone, J. F.; Colvin, V. L. J. Am. Chem. Soc. 1999, 121, 11630.
(36) Park, S. H.; Xia, Y. N. Chem. Mater. 1998, 10, 1745.
(37) Cassagneau, T.; Caruso, F. Adv. Mater. 2002, 14, 34.
(38) Jiang, P.; McFarland, M. J. J. Am. Chem. Soc. 2004, 126, 13778.
(39) Miguez, H.; Meseguer, F.; Lopez, C.; Lopez-Tejeira, F.; Sanchez-Dehesa, J. Adv. Mater. 2001, 13, 393.
(40) Bunz, U. H. F. Adv. Mater. 2006, 18, 973-989.
(41) Stenzel, M. H.; Barner-Kowollik, C.; Davis, T. P. J. Polym. Sci. Part A: Polym. Chem. 2006, 44, 2363-2375.
(42) Saunders, A. E.; Dickson, J. L.; Shah, P. S.; Lee, M. Y.; Lim, K. T.; Johnston, K. P.; Korgel, B. A. Physical Review 2006, 73, 031608.
(43) Madej, W.; Budkowski, A.; Raczkowska, J.; Rysz, J. Langmuir 2008, 24, 3517-3524.
(44) Zhao, B.; Zhang, J.; Wang, X.; Li, C. J. Mater. Chem. 2006, 16, 509-513.
(45) Wu, X. H.; Wang, S. F. ACS Appl. Mater. Interfaces 2012, 4, 4966.
(46) Sunami, H.; Ito, E.; Tanaka, M.; Yamamoto, S.; Shimomura, M. Colloids Surf. A 2006, 284, 548.
(47) Yamamoto, S.; Tanaka, M.; Sunami, H.; Arai, K.; Takayama, A.; Yamashita, S.; Motita, Y.; Shimomura, M. Surf. Sci. 2006, 600, 3785.
(48) Ke, B. B.; Wang, L. S.; Xu, Z. K. Langmuir 2010, 26,8946.
(49) Hernandez-Guerrero, M.; Min, E.; Barner-Kowollik, C.; Muller, A. H. E.; Stenzel, M. H. J. Mater. Chem. 2008, 18, 4718.

(50) Min, E. H.; Wong, K. H.; Stenzel, M. H. Adv. Mater. 2008, 20, 3550.
(51) Tanaka, M.; Takayama, A.; Ito, E.; Sunami, H.; Yamamoto, S.; Shimomura, M. J. Nanosci. Nanotechnol. 2007, 7, 763-772.
(52) Curtis, A.; Wilkinson, C. Biomaterials 1997, 18, 1573
(53) Mcmillan, J. R.; Akiyama, M.; Tanaka, M.; Yamamoto, S.; Goto, M.; Abe, R.; Sawamura, D.; Shimomura, M.; Shimizu, H. Tissue Eng. 2007, 13, 789.
(54) Orita, T.; Tomita, M.; Kato, K. Colloids Surf. B 2011, 84, 187.
(55) Wan, Y.; Wang, Y.; Liu, Z.; Qu, X.; Han, B.; Bei, J.; Wang, S. Biomaterials 2005, 26, 4453.
(56) Fukuhira, Y.; Kaneko, H.; Yamaga, M.; Tanaka, M.; Yamamoto, S.; Shimomura, M. Colloids Surf. A 2008, 313-314, 520.
(57) Schmidt, C. E.; Leach, J. B. Annu. Rev. Biomed. Eng. 2003, 5, 293..
(58) Cai, L.; Zhang, L.; Dong, J.; Wang, S. Langmuir 2012, 28, 12557.
(59) Hoffman-Kim, D.; Mitchel, J. A.; Bellamkonda, R. V. Annu. Rev. Biomed. Eng. 2010, 12, 203.
(60) Tsuruma, A.; Tanaka, M.; Yamamoto, S.; Shimomura, M. Colloids Surf. A 2008, 313-314, 536.
(61) Woo, S.; Gomez, T. M. J. Neurosci. 2006, 26, 1418.
(62) Ferrari, A.; Faraci, P.; Cecchini, M.; Beltram, F. Biomaterials 2010, 31, 2565.
(63) Huang, C.; Borchers, C. H.; Schaller, M. D.; Jacobson, K. J. Cell Biol. 2004, 164, 593.
(64) Allen, J.; Chilton, J. K. Dev. Biol. 2009, 327, 4.
(65) Rompre, P.; Auger, F. A.; Germain, L.; Bouvard, V.; Lopez Valle, C. A.; Thibault, J.; Le Duy, A. In Vitro Cell Dev Biol 1990, 26, 983.
(66) Tanaka, M.; Nishikawa, K.; Okubo, H.; Kamashi, H.; Kawai, T.; Matsushita, M.; Todo, S.; Shimomura, M. Colloids Surf. A 2006, 284-285, 464.
(67) Hall, A. Science 1998, 279, 509.
(68) Wang, B.; Mao, Z.; Meng, X.; Tong, W.; Gao, C. Colloids Surf. B 2010, 76, 38.
(69) Fukuhira, Y.; Kitazono, E.; Hayashi, T.; Kaneko, H.; Tanaka, M.; Shimomura, M.; Sumi, Y. Biomaterials 2006, 27, 1797.

.